ARTICLE

doi:10.1038/nature10722

A sensing array of radically coupled genetic 'biopixels'

Arthur Prindle[1]*, Phillip Samayoa[2]*, Ivan Razinkov[1], Tal Danino[1], Lev S. Tsimring[3] & Jeff Hasty[1,2,3,4]

Although there has been considerable progress in the development of engineering principles for synthetic biology, a substantial challenge is the construction of robust circuits in a noisy cellular environment. Such an environment leads to considerable intercellular variability in circuit behaviour, which can hinder functionality at the colony level. Here we engineer the synchronization of thousands of oscillating colony 'biopixels' over centimetre-length scales through the use of synergistic intercellular coupling involving quorum sensing within a colony and gas-phase redox signalling between colonies. We use this platform to construct a liquid crystal display (LCD)-like macroscopic clock that can be used to sense arsenic via modulation of the oscillatory period. Given the repertoire of sensing capabilities of bacteria such as *Escherichia coli*, the ability to coordinate their behaviour over large length scales sets the stage for the construction of low cost genetic biosensors that are capable of detecting heavy metals and pathogens in the field.

Synthetic biology can be broadly broken down into the 'top-down' synthesis of genomes[1] and the 'bottom-up' engineering of relatively small genetic circuits[2–10]. In the field of genetic circuits, toggle switches[11] and oscillators[12] have progressed into triggers[13], counters[14] and synchronized clocks[15]. Sensors have arisen as a major focus in the context of biotechnology[6,16,17], while oscillators have provided insights into the basic-science functionality of cyclic regulatory processes[18–20]. A common theme is the concurrent development of mathematical modelling that can be used for experimental design and characterization, as in physics and the engineering disciplines.

The synchronization of genetic clocks provides a particularly attractive avenue for synthetic biology applications. Oscillations permeate science and technology in a number of disciplines, with familiar examples including alternating current (AC) power[21], the global positioning system (GPS)[22] and lasers[23]. These technologies have demonstrated that operating in the frequency domain can offer considerable advantages over steady-state designs in terms of information gathering and transmission. In particular, oscillatory sensors confer a number of advantages to traditional ones[24], as frequency is easily digitized and can be quickly updated with repeated measurements. For sensors that use optical reporters, measurements of frequency are less sensitive to experimental factors such as beam power and exposure time than intensity measurements, which must be normalized and calibrated.

Although the bottom-up approach to synthetic biology is increasingly benefiting from DNA synthesis technologies, the general design principles are still evolving. In this context, a substantial challenge is the construction of robust circuits in a cellular environment that is governed by noisy processes such as random bursts of transcription and translation[25–29]. Such an environment leads to considerable intercellular variability in circuit behaviour, which can impede coherent functionality at the colony level. An ideal design strategy for reducing variability across a cellular population would involve both strong and long-range coupling that would instantaneously synchronize the response of millions of cells. Quorum sensing typically involves strong intercellular coupling over tens of micrometres[8,15,30], yet the relatively slow diffusion time of molecular communication through cellular media leads to signalling delays over millimetre scales. Faster communication mechanisms, such as those mediated in the gas phase, may increase the length scale for instantaneous communication, but are comparatively weak and short lived because the vapour species more readily disperse.

Synergistic synchronization

To develop a frequency-modulated biosensor, we designed a gene network capable of synchronizing genetic oscillations across multiple scales (Fig. 1a and Supplementary Fig. 1). We constructed an LCD-like microfluidic[31] array that allows many separate colonies of sensing bacteria to grow and communicate rapidly by gas exchange (Fig. 1b, c and Supplementary Fig. 9). As previous work[15] has demonstrated that coupling through quorum sensing leads to incoherent oscillations at the millimetre scale, this mode of cellular communication is too slow for the generation of macroscopic synchronized oscillations. However, the slower quorum sensing can be used to synchronize small local colonies, provided there is a second level of design that involves faster communication for coordination between the colonies. Therefore, rather than attempting to engineer a sensor from a single large-colony oscillator, we wired together thousands of small oscillating colonies, or 'biopixels', in a microfluidic array. Coupling between biopixels involves redox signalling by hydrogen peroxide (H_2O_2) and the native redox sensing machineries of *E. coli*. The two coupling mechanisms act synergistically in the sense that the stronger, yet short-range, quorum sensing is necessary to coherently synchronize the weaker, yet long-range, redox signalling. Using this method we demonstrate synchronization of approximately 2.5 million cells across a distance of 5 mm, over 1,000 times the length of an individual cell (Fig. 1c, d and Supplementary Movies 1 and 2). This degree of synchronization yields extremely consistent oscillations, with a temporal accuracy of about 2 min compared to 5–10 min for a single oscillator[15] (Fig. 1d).

The global synchronization mechanism is comprised of two modes of communication that work on different scales. The quorum-sensing

[1]Department of Bioengineering, University of California, San Diego, La Jolla, California 92093, USA. [2]Bioinformatics Program, University of California, San Diego, La Jolla, California 92093, USA. [3]BioCircuits Institute, University of California, San Diego, La Jolla, California 92093, USA. [4]Molecular Biology Section, Division of Biological Science, University of California, San Diego, La Jolla, California 92093, USA.
*These authors contributed equally to this work.

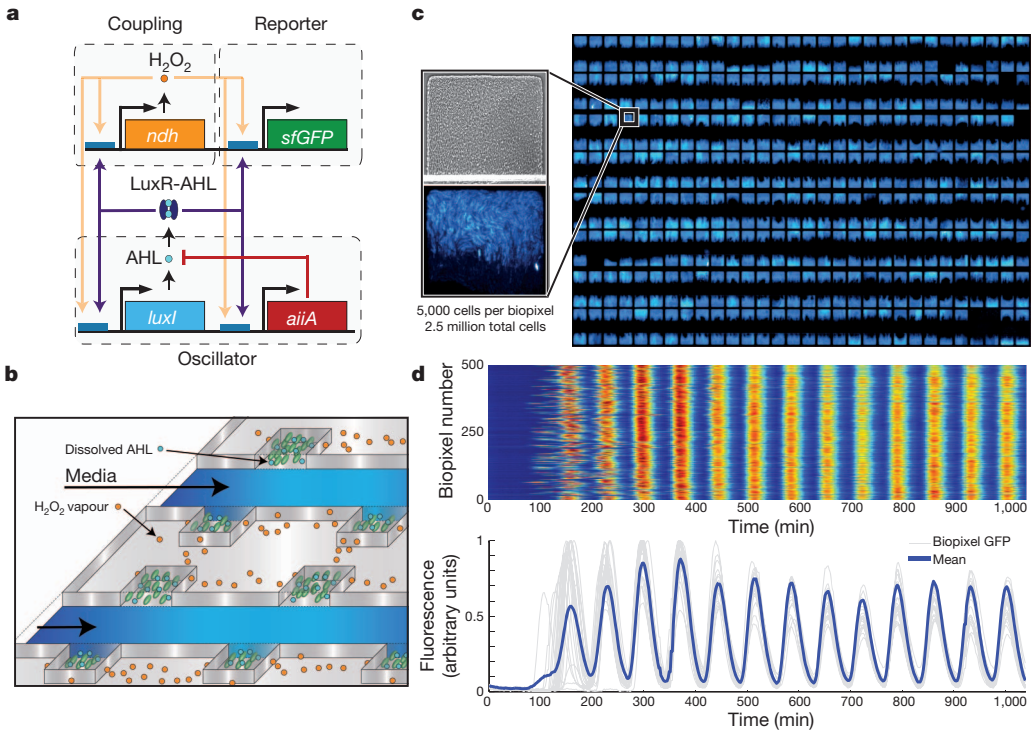

Figure 1 | Sensing array of radically coupled genetic biopixels. **a**, Network diagram. The *luxI* promoter drives expression of *luxI*, *aiiA*, *ndh* and *sfGFP* (superfolder variant of GFP) in four identical transcription modules. The quorum-sensing genes *luxI* and *aiiA* generate synchronized oscillations within a colony via AHL. The *ndh* gene codes for NDH-2, an enzyme that generates H_2O_2 vapour, which is an additional activator of the *luxI* promoter. H_2O_2 is capable of migrating between colonies and synchronizing them. **b**, Conceptual design of the sensing array. AHL diffuses within colonies while H_2O_2 migrates between adjacent colonies through the PDMS. Arsenite-containing media is passed in through the parallel feeding channels. **c**, Fluorescent image of an array of 500 *E. coli* biopixels containing about 2.5 million cells. Inset, bright-field and fluorescent images display a biopixel of 5,000 cells. **d**, Heat map and trajectories depicting time-lapse output of 500 individual biopixels undergoing rapid synchronization. Sampling time is 2 min.

machinery (LuxI, AiiA) uses an acyl-homoserine lactone (AHL) to mediate intracolony synchronization. In our device, the degree to which neighbouring colonies are able to influence each other via AHL diffusion is negligible owing to the high media channel flow rates. Instead, we engineered the cells to communicate via gas exchange by placing a copy of the gene coding for NADH dehydrogenase II (*ndh*) under the control of an additional *lux* promoter. NDH-2 is a membrane-bound respiratory enzyme that produces low levels of H_2O_2 and superoxide (O_2^-)[32]. As H_2O_2 vapour is able to pass through the 25-μm oxygen-permeable polydimethylsiloxane (PDMS) walls that separate adjacent colonies, periodic production of NDH-2 yields periodic exchange of H_2O_2 between biopixels. When H_2O_2 enters the cell, it transiently changes its redox state, interacting with our synthetic circuit through the native aerobic response control systems, including ArcAB, which has a binding site in the *lux* promoter region[33,34]. Under normal conditions, ArcAB is partially active so *lux* is partially repressed. In contrast, oxidizing conditions triggered by H_2O_2 inactivate ArcAB, relieving this repression. Each oscillatory burst promotes firing in neighbouring colonies by relieving repression on the *lux* promoter. This constitutes an additional positive feedback that rapidly synchronizes the population (Supplementary Fig. 2 and Supplementary Movie 1).

We investigated the effects of catalase and superoxide dismutase (SOD) to probe the nature of H_2O_2 communication. When a population of synchronized colonies was exposed to a step increase of 200 U ml^{-1} catalase, an enzyme that rapidly degrades extracellular H_2O_2[35], synchronization was broken and colonies continued to oscillate individually (Supplementary Fig. 3). As the cell membrane is impermeable to catalase, asynchronous colony oscillations confirm that communication between colonies depends on external H_2O_2 whereas oscillations within a colony do not. Conversely, when we enhanced the rate of superoxide conversion to H_2O_2 by expressing *sodA*[36,37] from an additional *lux* promoter, colonies quickly fired in a spatial wave and failed to oscillate further despite no changes to growth rate or cell viability (Supplementary Fig. 4). Because H_2O_2 is produced internal to the cell, this confirms that H_2O_2 is capable of escaping the cell and activating *lux*-regulated genes in neighbouring colonies via diffusion. The apparent higher output of H_2O_2 by SOD as compared to NDH-2 is probably due to its very high catalytic efficiency[38]. Lastly, we observed synchronization between arrays of traps even when they were fluidically isolated but held in close proximity (Supplementary Fig. 5). These devices share no common fluid sources or channels, making communication by dissolved molecules like AHL impossible. Taken together, these results confirm that gaseous H_2O_2 is the mode of communication between oscillating colonies.

On the basis of our understanding of the mechanism for global synchronization, we expected that we could simplify the circuitry by eliminating *ndh* and achieve the same effect with intermittent bursts of high-intensity blue light. In this design, the GFP molecule acts as a photosensitizer, releasing free radicals upon exposure that produce reactive oxygen species (ROS) including H_2O_2[39]. At the peak of oscillation, considerable vapour-phase H_2O_2 is produced by exposing GFP-containing cells to fluorescent light. Conversely, at the trough of oscillation, cells contain almost no GFP, and therefore produce very little H_2O_2 upon fluorescing. Bursts of light thus generate bursts of H_2O_2 vapour whose concentration depends on the oscillating GFP level, just as periodic production of NDH-2 did previously. Indeed, this strategy was similarly able to synchronize our sensor array (Fig. 1d and Supplementary Movie 2). Numerous controls were performed to ensure that synchronized oscillations did not occur at low fluorescence intensities (Supplementary Fig. 6 and Supplementary Movie 9).

To probe this mode of synchronization, we investigated the effects of thiourea and the antibiotics ampicillin and kanamycin. When a synchronized population of colonies was exposed to 35 mM thiourea, a

potent radical quencher[40,41], we observed sharply decaying synchronized oscillations whereas growth rate and cell viability were unaffected (Supplementary Fig. 7). This suggests that without radical species, oscillations cannot be produced. Next, we ran a series of experiments switching the antibiotic resistance genes on our plasmids. We noted that radical-producing antibiotics[42], particularly ampicillin, significantly reduced the degree of synchronization, showing that an excess of radical species also hinders communication (Supplementary Fig. 8). As our final constructs included a plasmid with kanamycin resistance, which was also found to produce some radicals, we used full (50 μg ml^{-1}) selection when growing up the cells but very low (5 μg ml^{-1}) selection during the experimental run. Persistence of oscillations, sequencing, and subsequent growth in full selection following the run confirmed the presence of all three plasmids despite this low experimental selection. Catalase and SOD results were identical to those with NDH-2 synchronization (not shown). These results show that fluorescence-mediated synchronization involves the production of radical species after fluorescence exposure and communication via H_2O_2.

Sensing array of biopixels

With a platform for generating consistent and readily detectable oscillations, we sought to use the circuit to engineer an arsenic-sensing macroscopic biosensor. We rewired the network to include an extra copy of the positive-feedback element, the AHL synthase LuxI, under the control of a native arsenite-responsive promoter that is repressed by ArsR in the absence of arsenite (Fig. 2a, right). When arsenite is not present in the media, supplementary *luxI* is not transcribed and the circuit functions normally, generating baseline oscillations. However, the addition of trace amounts of arsenite relieves this repression and allows supplementary *luxI* to be transcribed, increasing the oscillatory amplitude and period. Tuning the level of LuxI by varying arsenite concentration results in clear changes to the oscillatory period (Fig. 2b and Supplementary Movie 2). To determine the range of detection, we swept arsenite concentrations from 0–1 μM and measured the oscillatory period (Fig. 2c, top). Using statistical methods (Supplementary Methods), we generated a sensor calibration curve (Fig. 2c, bottom) that depicts the maximum possible arsenite concentration present ($\alpha = 95\%$) for a given measured period. This curve is an illustration of how data generated by our array would be used to measure arsenite concentrations in an unknown sample using our device. Our system was able to reliably quantify arsenite levels as low as 0.2 μM, below the 0.5 μM World Health Organization-recommended level for developing nations[43].

As an alternative sensing strategy, we rewired the network to include a copy of the *luxR* gene controlled by an arsenite-responsive promoter while removing it from the rest of the circuit (Fig. 2a, left). Because the LuxR–AHL complex must be present to activate the *lux* promoter[30], cells produce no LuxR when the media is free of arsenite, generating no fluorescence or oscillations. The addition of arsenite stimulates the production of LuxR, restoring circuit function and producing clear, synchronized oscillations (Fig. 2d and Supplementary Movie 3). This ON/OFF detection system has a threshold of 0.25 μM, a detection limit that can be adjusted by changing the copy number, ribosome binding site (RBS) strength, or promoter strength of the sensing plasmid (Supplementary Methods).

The sensing array is also capable of producing complex behaviours arising from the dynamic interaction of cellular colonies. By making modifications to the size, number and arrangement of biopixels in the device, we are able to markedly alter the output waveforms. For

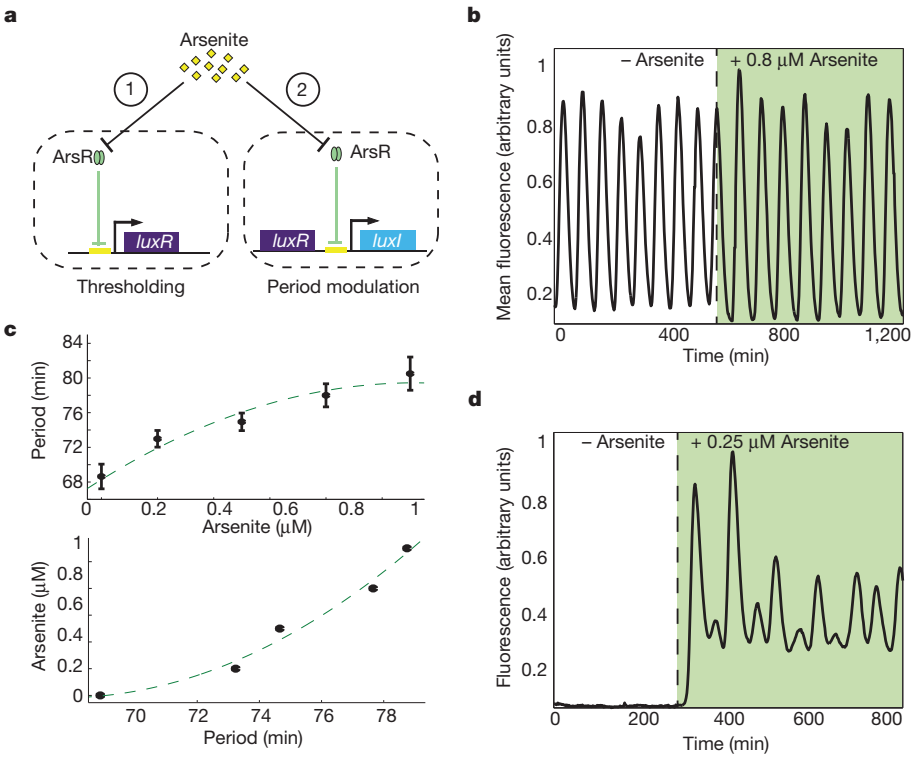

Figure 2 | Frequency-modulated genetic biosensor. **a**, Network diagrams depicting two constructed sensing modules. In thresholding (1), the *luxR* gene is removed from the oscillator network and supplemented by a new copy driven by an arsenite-responsive promoter. In period modulation (2), a supplementary *luxI* gene tagged for increased degradation is driven by the arsenic-responsive promoter, which affects the period of oscillation. **b**, A sample period modulation sensor output following a step increase of 0.8 μM arsenite. Oscillatory period increases from 69 min to 79 min. **c**, Top, period versus arsenite concentration for the sensor array. Error bars indicate ± 1 standard deviation averaged over 500 biopixel trajectories. Dotted line represents model-predicted curve. Bottom, sensor calibration curve generated from experimental data. Points indicate the maximum arsenite level with 95% certainty for a given measured period as determined statistically from experimental data. **d**, Thresholder output following a step increase of 0.25 μM arsenite. A marked shift from rest to oscillatory behaviour is observed within 20 min after the addition of arsenite.

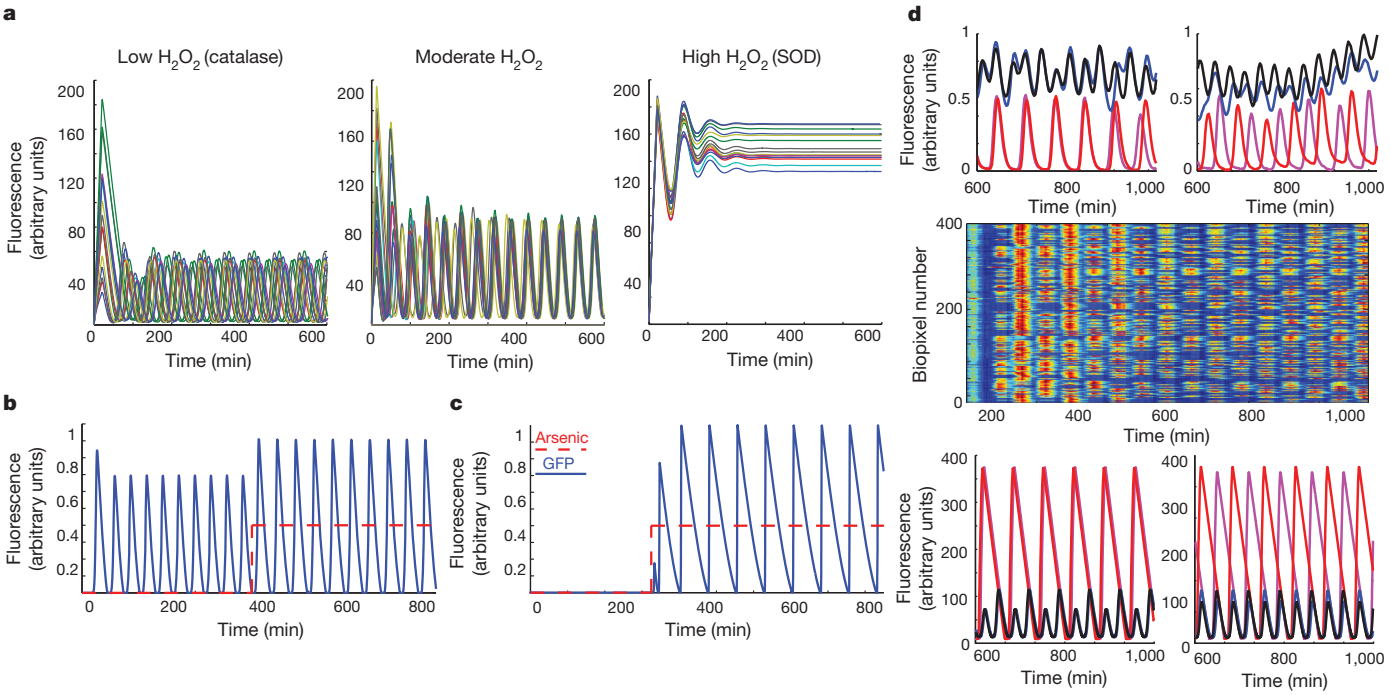

Figure 3 | Computational modelling of radical synchronization and biosensing. **a**, Time series of a population of biopixels producing varying amounts of H_2O_2 vapour. Synchronization occurs only for moderate levels whereas high levels lock ON and low levels oscillate asynchronously. **b**, A typical time series for our period modulation sensor undergoing a step increase of arsenite. Oscillations increase in both amplitude and period. **c**, A typical time series output for the thresholding sensor. Oscillations arise after the addition of arsenite. **d**, Experimental and computational output depicting complex dynamic behaviours between neighbouring traps. Top, 1:2 resonance and anti-phase synchronization observed when trap size (left, black/blue = 95 μm depth and red/magenta = 85 μm depth) and separation distance (right, same colours) are modified experimentally. Middle, scaled-up array experimental data for increased trap separation experiments demonstrating anti-phase synchronization. Bottom, computational model trajectories depicting 1:2 resonance and anti-phase synchronization when trap size (same colours as experimental data) and separation distance are changed.

example, when we constructed a device in which trap separation distance is increased (45 μm versus 25 μm), we observed local anti-phase synchronization between neighbouring colonies (Fig. 3d, top right). To explore this phenomenon on a larger scale, we constructed a device that contains an array of 416 traps constructed according to the specifications above. In these experiments, we observe initial global synchronization that gradually falls into local anti-phase synchronization across the array (Fig. 3d, middle. and Supplementary Movie 4). Phase alignment is maintained over at least 48 h, with patches of synchronization typically 3–6 colonies in size. Alternatively, by changing dimensions such that the array contains traps of two slightly different sizes, we observe a 1:2 resonance synchronization where larger traps pulse at double the frequency of smaller traps while maintaining synchronization (Fig. 3d, top left and Supplementary Movie 7). Lastly, when LuxR is limited, as in the thresholding scheme, we observe synchronized oscillations of alternating large and small peaks in both experiment and model (Supplementary Fig. 12). Our computational model (Box 1) captures these effects (Fig. 3d, bottom, and Supplementary Figs 11 and 12) and indicates that further array manipulation will yield new, richer dynamics that could not be produced directly by changing circuit structure.

Although our sensor array is capable of performing a variety of complex functions in the laboratory, adapting this technology to a real-world device will require the elimination of the expensive and bulky microscopy equipment. However, measuring genetic oscillations in the absence of any magnification or powerful illumination will require an even further increased signal. Using this mechanism of global synchronization, we were able to scale up to a 24 mm × 12 mm array that houses over 12,000 communicating biopixels (Fig. 4a). Synchronization is maintained across the entire array, a distance over 5,000 times the length of an individual cell, using an inexpensive light-emitting diode (LED; Fig. 4b, c and Supplementary Movie 5). The signal strength generated by the large number of cells in the array (about 50 million) will allow us to adapt the device to function as a handheld sensor. In our conceptual design (Fig. 4d), the sensor will

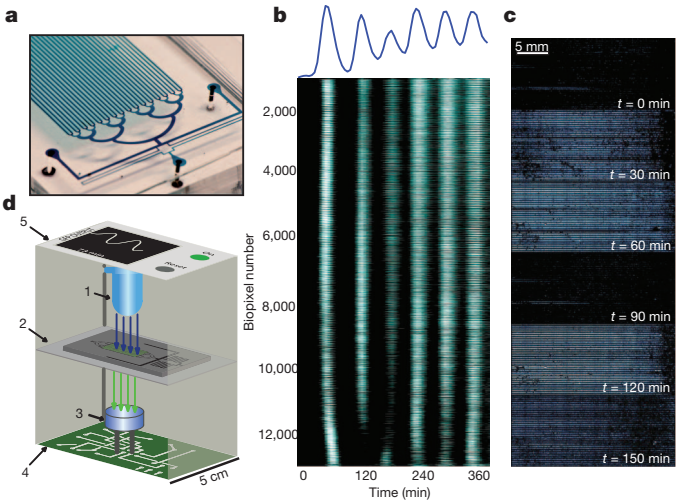

Figure 4 | Radical synchronization on a macroscopic scale. **a**, The scaled-up array is 24 mm × 12 mm and houses over 12,000 biopixels that contain approximately 50 million total cells when filled. **b**, Global synchronization is maintained across the array. Heat map of individual trajectories of all 12,224 oscillating biopixels. **c**, Image series depicting global synchronization and oscillation for the macroscopic array. Each image is produced by stitching 72 fields of view imaged at ×4 magnification. **d**, Schematic diagram illustrating our design for a handheld device using the sensing array. An LED (1) excites the array (2) and emitted light is collected by a photodetector (3), analysed by an onboard processor (4), and displayed graphically (5).

BOX 1

Computational modelling

Our model of the frequency-modulated biosensor is based on a previously described model for the quorum-sensing synchronized oscillator[15]. In addition to the reactions reflected in that model, we include the arsenite-induced production and degradation of LuxI and/or LuxR. From the biochemical reactions, we derived a set of delay-differential equations to be used as our model. These delayed reactions mimic the complex cascade of processes (transcription, translation, maturation, etc.) leading to formation of functional proteins. As expected, our model predicts oscillations that change frequency when changes in arsenite occur (Figs 2c and 3b). The amplitude and period of the oscillations both depend on the concentrations of the toxin. We then modified the model to describe the LuxR-based detection system. Our model predicts a marked transition from rest to oscillations upon addition of arsenite, consistent with experimental observations (Fig. 3c).

The multi-scale nature of communication in our array allows us to treat colony and array-level dynamics separately; in the latter, arsenite affects the quorum-sensing machinery of a colony, producing changes to oscillatory period that propagate between biopixels in the array. To describe quantitatively the mechanisms driving synchronization at the array level, we treat each colony as a single oscillator that acts according to degrade-and-fire kinetics[47]. We also include the production of H_2O_2 and its interaction with neighbouring colonies by two-dimensional diffusion. Using this model we identified three regimes that correlate well with experimental observations (Fig. 3a). When the effective production of H_2O_2 is low, as with catalase, we observe unsynchronized oscillations owing to constant, mild repression of the *lux* promoter via ArcAB (Fig. 3a, left). In contrast, when H_2O_2 production is very high, neighbouring colonies rapidly fire in succession and remain on because of the permanent activation of the *lux* promoter, consistent with the SOD experiment (Fig. 3a, right). Finally, at intermediate H_2O_2, we observe globally synchronized oscillations (Fig. 3a, middle). As colonies are moved further apart, synchronicity breaks owing to slowed migration of H_2O_2 (Supplementary Fig. 10).

continuously read the oscillatory frequency using off-the-shelf electronic components costing less than 50 dollars.

There have been many examples of bacteria-based biosensors[44–46], usually involving an optical reporter driven by a toxin-responsive promoter. Because optical intensity readings are sensitive to imaging conditions like beam power and exposure time, measurements must typically be normalized and calibrated. Measuring the period of oscillation allows us to avoid these issues because peak-to-peak time does not depend on individual peak intensity. Also, oscillations produced at the colony level effectively decouple the signal from the growth state of individual cells, which can also affect fluorescence intensity. By using a dynamic readout that depends on communication between biopixels, we scan and tune potential output signals by changing device parameters rather than redesigning the underlying circuit. For example, we might design a new sensing scheme in which oscillations synchronize with the addition of some toxin and shift to anti-phase or resonant synchronization when critical toxin levels are present.

Scaling up synthetic biology

By nesting two modes of communication we are able to expand the scale over which individual cells are coordinated and increase the complexity of their interaction. Indeed, there are many familiar examples of hierarchical systems. Airline routes are often designed such that small airports are connected locally to larger hubs that are connected internationally. It would neither be feasible nor desirable to connect every airport together. Similarly, individual cells communicate locally by one method, generating impulses large enough to enable colonies to communicate globally by another. Nesting communication mechanisms in this way may allow us to better scale up synthetic circuits of different types, such as switches and logic gates, paving the way for the next generation of synthetic biology pursuits.

METHODS SUMMARY

Strains and plasmids. The plasmids were constructed using a PCR-based cloning strategy[48] in which the origin of replication, antibiotic resistance, and circuit genes were assembled in different combinations. The *ndh* and *sodA* genes were amplified directly from the native *E. coli* genome by PCR. Various arsenite-responsive promoters were tested, including a recently reported synthetic version[49], but the final design uses the native *E. coli* version. Promoter output was tuned by changing the RBS sequence and quantified using flow cytometry. All circuit components except *luxR* were tagged by PCR with a carboxy-terminal *ssrA* tag (AANDENYALAA)[50] for fast degradation.

Microfluidics and microscopy. Image acquisition was performed on a Nikon Eclipse TI epifluorescent inverted microscope outfitted with fluorescence filter cubes optimized for GFP imaging and a phase-contrast-based autofocus algorithm. Images were acquired using an Andor Clara cooled CCD camera or Andor DU-897 EMCCD camera, both controlled by Nikon Elements software. Images were acquired every 2 min in phase contrast and fluorescence. The cells were imaged inside a microfluidic device with an upstream switch, with the ability to mix or switch between two different media sources. A custom application written in LabVIEW (National Instruments) controlled linear actuators, to which two reservoirs of arsenite-containing and pure medium were attached. Using this algorithm, arsenite concentration was dynamically varied to probe sensor output.

The microfluidic experiments were performed as previously described[15]. Briefly, 50 µl of an overnight culture was diluted in 50 ml of LB medium (Difco) plus antibiotics the day of the experiment. When cells reached an optical density ($OD_{600\,nm}$) of 0.1, cells were spun down and resuspended in 5 ml of fresh media and loaded into the device.

Received 2 September; accepted 15 November 2011.
Published online 18 December 2011.

1. Gibson, D. *et al.* Creation of a bacterial cell controlled by a chemically synthesized genome. *Science* **329,** 52–56 (2010).
2. Hasty, J., McMillen, D. & Collins, J. J. Engineered gene circuits. *Nature* **420,** 224–230 (2002).
3. Sprinzak, D. & Elowitz, M. B. Reconstruction of genetic circuits. *Nature* **438,** 443–448 (2005).
4. Endy, D. Foundations for engineering biology. *Nature* **438,** 449–453 (2005).
5. Ellis, T., Wang, X. & Collins, J. Diversity-based, model-guided construction of synthetic gene networks with predicted functions. *Nature Biotechnol.* **27,** 465–471 (2009).
6. Kobayashi, H. *et al.* Programmable cells: interfacing natural and engineered gene networks. *Proc. Natl Acad. Sci. USA* **101,** 8414–8419 (2004).
7. You, L., Cox, R. S. III, Weiss, R. & Arnold, F. H. Programmed population control by cell–cell communication and regulated killing. *Nature* **428,** 868–871 (2004).
8. Basu, S., Gerchman, Y., Collins, C. H., Arnold, F. H. & Weiss, R. A synthetic multicellular system for programmed pattern formation. *Nature* **434,** 1130–1134 (2005).
9. Mukherji, S. & Van Oudenaarden, A. Synthetic biology: understanding biological design from synthetic circuits. *Nature Rev. Genet.* **10,** 859–871 (2009).
10. Grilly, C., Stricker, J., Pang, W., Bennett, M. & Hasty, J. A synthetic gene network for tuning protein degradation in *Saccharomyces cerevisiae*. *Mol. Syst. Biol.* **3,** 127 (2007).
11. Gardner, T. S., Cantor, C. R. & Collins, J. J. Construction of a genetic toggle switch in *Escherichia coli*. *Nature* **403,** 339–342 (2000).
12. Elowitz, M. B. & Leibler, S. A synthetic oscillatory network of transcriptional regulators. *Nature* **403,** 335–338 (2000).
13. Lu, T. & Collins, J. Dispersing biofilms with engineered enzymatic bacteriophage. *Proc. Natl Acad. Sci. USA* **104,** 11197–11202 (2007).
14. Friedland, A. *et al.* Synthetic gene networks that count. *Science* **324,** 1199–1202 (2009).
15. Danino, T., Mondragon-Palomino, O., Tsimring, L. & Hasty, J. A synchronized quorum of genetic clocks. *Nature* **463,** 326–330 (2010).
16. Tamsir, A., Tabor, J. & Voigt, C. Robust multicellular computing using genetically encoded NOR gates and chemical 'wires'. *Nature* **469,** 212–215 (2011).
17. Tabor, J. *et al.* A synthetic genetic edge detection program. *Cell* **137,** 1272–1281 (2009).
18. Stricker, J. *et al.* A fast, robust and tunable synthetic gene oscillator. *Nature* **456,** 516–519 (2008).
19. Mondragon-Palomino, O., Danino, T., Selimkhanov, J., Tsimring, L. & Hasty, J. Entrainment of a population of synthetic genetic oscillators. *Science* **333,** 1315–1319 (2011).
20. Tigges, M., Marquez-Lago, T., Stelling, J. & Fussenegger, M. A tunable synthetic mammalian oscillator. *Nature* **457,** 309–312 (2009).

21. Westinghouse, G. System of electrical distribution. US patent 373 035 (1887).
22. Lewandowski, W., Azoubib, J. & Klepczynski, W. GPS: primary tool for time transfer. *Proc. IEEE* **87,** 163–172 (1999).
23. Vladimirov, A., Kozyreff, G. & Mandel, P. Synchronization of weakly stable oscillators and semiconductor laser arrays. *Europhys. Lett.* **61,** 613 (2003).
24. Gast, T. Sensors with oscillating elements. *J. Phys. E: Sci. Instrum.* **18,** 783 (1985).
25. Ozbudak, E. M., Thattai, M., Kurtser, I., Grossman, A. D. & van Oudenaarden, A. Regulation of noise in the expression of a single gene. *Nature Genet.* **31,** 69–73 (2002).
26. Elowitz, M. B., Levine, A. J., Siggia, E. D. & Swain, P. S. Stochastic gene expression in a single cell. *Science* **297,** 1183–1186 (2002).
27. Golding, I., Paulsson, J., Zawilski, S. & Cox, E. Real-time kinetics of gene activity in individual bacteria. *Cell* **123,** 1025–1036 (2005).
28. Blake, W. *et al.* Phenotypic consequences of promoter-mediated transcriptional noise. *Mol. Cell* **24,** 853–865 (2006).
29. Austin, D. *et al.* Gene network shaping of inherent noise spectra. *Nature* **439,** 608–611 (2006).
30. Waters, C. & Bassler, B. Quorum sensing: cell-to-cell communication in bacteria. *Annu. Rev. Cell Dev. Biol.* **21,** 319–346 (2005).
31. Ferry, M., Razinkov, I. & Hasty, J. Microfluidics for synthetic biology from design to execution. *Methods Enzymol.* **497,** 295 (2011).
32. Messner, K. & Imlay, J. The identification of primary sites of superoxide and hydrogen peroxide formation in the aerobic respiratory chain and sulfite reductase complex of *Escherichia coli*. *J. Biol. Chem.* **274,** 10119–10128 (1999).
33. Bose, J. L. *et al.* Bioluminescence in *Vibrio fischeri* is controlled by the redox-responsive regulator arca. *Mol. Microbiol.* **65,** 538–553 (2007).
34. Georgellis, D., Kwon, O. & Lin, E. Quinones as the redox signal for the arc two-component system of bacteria. *Science* **292,** 2314–2316 (2001).
35. Seaver, L. & Imlay, J. Hydrogen peroxide fluxes and compartmentalization inside growing *Escherichia coli*. *J. Bacteriol.* **183,** 7182–7189 (2001).
36. Fridovich, I. The biology of oxygen radicals. *Science* **201,** 875–880 (1978).
37. McCord, J. & Fridovich, I. Superoxide dismutase. *J. Biol. Chem.* **244,** 6049–6055 (1969).
38. Berg, J., Tymoczko, J. L. & Stryer, L. *Biochemistry* (W.H. Freeman, 2006).
39. Remington, S. Fluorescent proteins: maturation, photochemistry and photophysics. *Curr. Opin. Struct. Biol.* **16,** 714–721 (2006).
40. Kelner, M., Bagnell, R. & Welch, K. Thioureas react with superoxide radicals to yield a sulfhydryl compound. explanation for protective effect against paraquat. *J. Biol. Chem.* **265,** 1306–1311 (1990).
41. Touati, D., Jacques, M., Tardat, B., Bouchard, L. & Despied, S. Lethal oxidative damage and mutagenesis are generated by iron in delta fur mutants of *Escherichia coli*: protective role of superoxide dismutase. *J. Bacteriol.* **177,** 2305–2314 (1995).
42. Kohanski, M. A., DePristo, M. A. & Collins, J. J. Sublethal antibiotic treatment leads to multidrug resistance via radical-induced mutagenesis. *Mol. Cell* **37,** 311–320 (2010).
43. Nordstrom, D. Worldwide occurrences of arsenic in ground water. *Science* **296,** 2143 (2002).
44. van der Meer, J. & Belkin, S. Where microbiology meets microengineering: design and applications of reporter bacteria. *Nature Rev. Microbiol.* **8,** 511–522 (2010).
45. Daunert, S. *et al.* Genetically engineered whole-cell sensing systems: coupling biological recognition with reporter genes. *Chem. Rev.* **100,** 2705–2738 (2000).
46. Leveau, J. & Lindow, S. Bioreporters in microbial ecology. *Curr. Opin. Microbiol.* **5,** 259–265 (2002).
47. Mather, W., Bennett, M., Hasty, J. & Tsimring, L. Delay-induced degrade-and-fire oscillations in small genetic circuits. *Phys. Rev. Lett.* **102,** 068105 (2009).
48. Quan, J. & Tian, J. Circular polymerase extension cloning of complex gene libraries and pathways. *PLoS ONE* **4,** e6441 (2009).
49. Stocker, J. *et al.* Development of a set of simple bacterial biosensors for quantitative and rapid measurements of arsenite and arsenate in potable water. *Environ. Sci. Technol.* **37,** 4743–4750 (2003).
50. Keiler, K., Waller, P. & Sauer, R. Role of a peptide tagging system in degradation of proteins synthesized from damaged messenger RNA. *Science* **271,** 990–993 (1996).

Supplementary Information is linked to the online version of the paper at www.nature.com/nature.

Acknowledgements This work was supported by the National Institutes of Health and General Medicine (R01GM69811), the San Diego Center for Systems Biology (P50GM085764), the DoD NDSEG (A.P.) and NSF Graduate Research (P.S.) Fellowship Programs. L.T. was supported, in part, by the Office of Naval Research (MURI N00014-07-0741). We would like to thank J. Imlay, S. Ali and J. Collins for helpful discussions and J. Hickman, B. Taylor and K. Lomax for their help with illustrations.

Author Contributions All authors contributed extensively to the work presented in this paper. A.P. and P.S. are equally contributing first authors.

Author Information Reprints and permissions information is available at www.nature.com/reprints. The authors declare no competing financial interests. Readers are welcome to comment on the online version of this article at www.nature.com/nature. Correspondence and requests for materials should be addressed to J.H. (hasty@bioeng.ucsd.edu).

doi:10.1038/nature10722

Plasmid Construction

The oscillator plasmids were constructed by modifying the constructs used in a previous study (1). The antibiotic resistance genes of pTD103AiiA was switched to chloramphenicol. The reporter protein on pTD103LuxI/GFP was switched to a recently reported superfolding green fluorescent protein, sfGFP (2). The ndh and sodA genes were amplified directly from the native *E. coli* genome by PCR. Promoter output was tuned by changing the RBS sequence and quantified using flow cytometry. We initially constructed the sensing plasmid with a published synthetic background-reduced version that contains additional ArsR operator sites(3) but failed to produce enough LuxR. To increase LuxR output, we reverted to the native promoter sequence, switched the RBS to that of pZ plasmids(**?**), and increased the copy number by a factor of 5 by switching to a mutated SC101 origin of replication. All circuit components except LuxR were tagged by PCR with a carboxy-terminal ssrA tag (AANDENYALAA) (4) for fast degradation. Modular pieces (resistance genes, promoters, origins, and ORFs) were assembled using a PCR-based cloning scheme named CPEC (5).

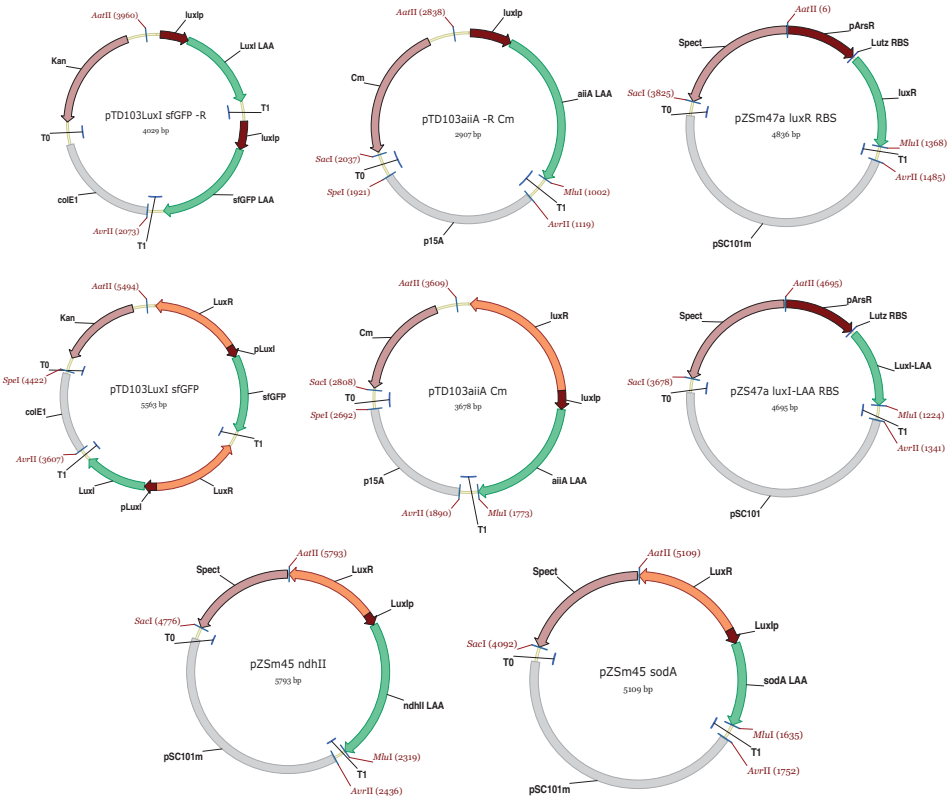

Supplementary Figure 1: Plasmids used in this study. Top row is the thresholding sensor: 2 oscillator plasmids with luxR genes removed and a plasmid containing pArs::luxR. Middle row is the period modulator: 2 oscillator plasmids and a plasmid containing pArs::luxI-laa. Bottom row contains 2 plasmids used to study H_2O_2 production and synchronization: pLux::ndh and pLux::sodA. NDH-2 synchronization strain is the oscillator plasmids with pZSm45 ndhII.

Additional Experimental Results

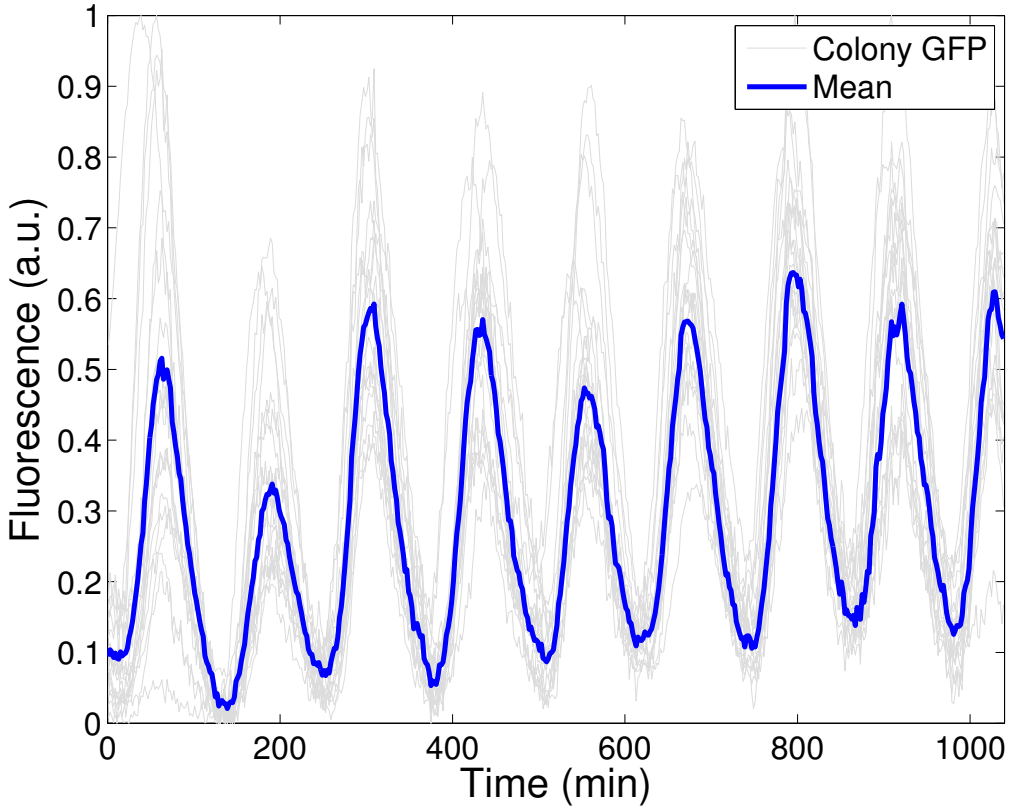

Supplementary Figure 2: Biopixels with NDH-2 engineered synchronization observed at ultra-low fluorescence (4X, 20ms exposure, 3% power) using an EMCCD camera to ensure no fluorescence interaction. Synchronized oscillations are maintained across the array for the length of the experiment (14 hours).

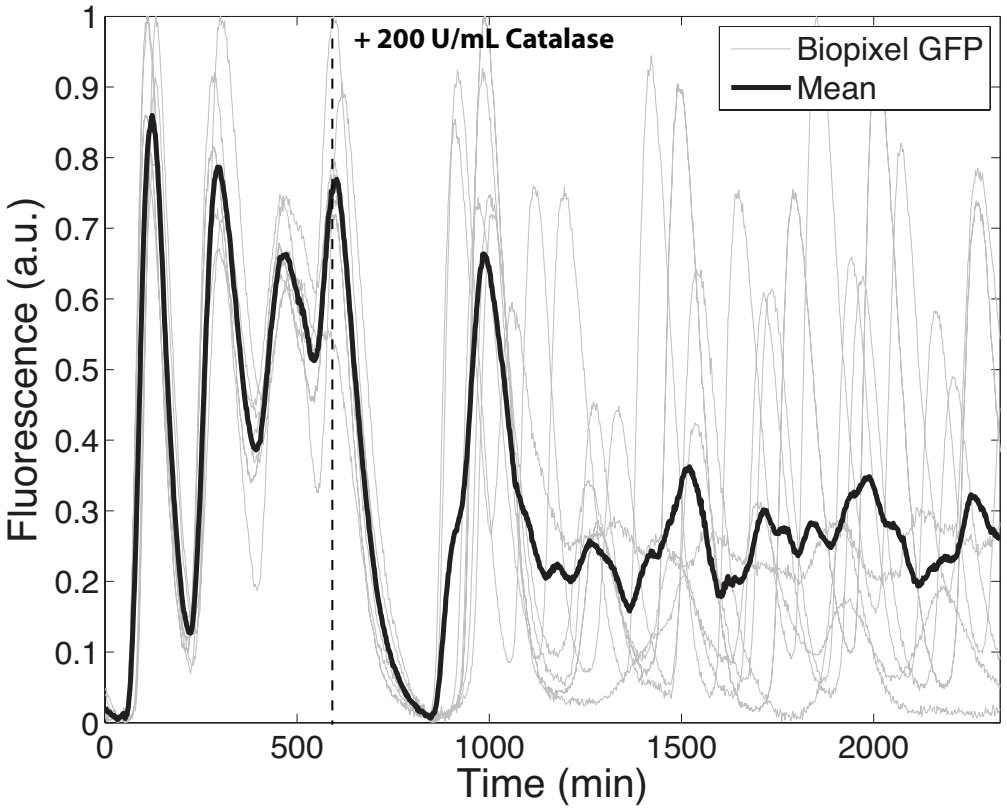

Supplementary Figure 3: Catalase degrades external H_2O_2 and prevents communication between colonies. When a synchronized population of biopixels was exposed to a step increase of 200 U/ml catalase, synchronization was broken and biopixels continued to oscillate individually. Since catalase can't cross the cell membrane, this shows that synchronization between colonies depends on H_2O_2 but oscillations with a colony do not.

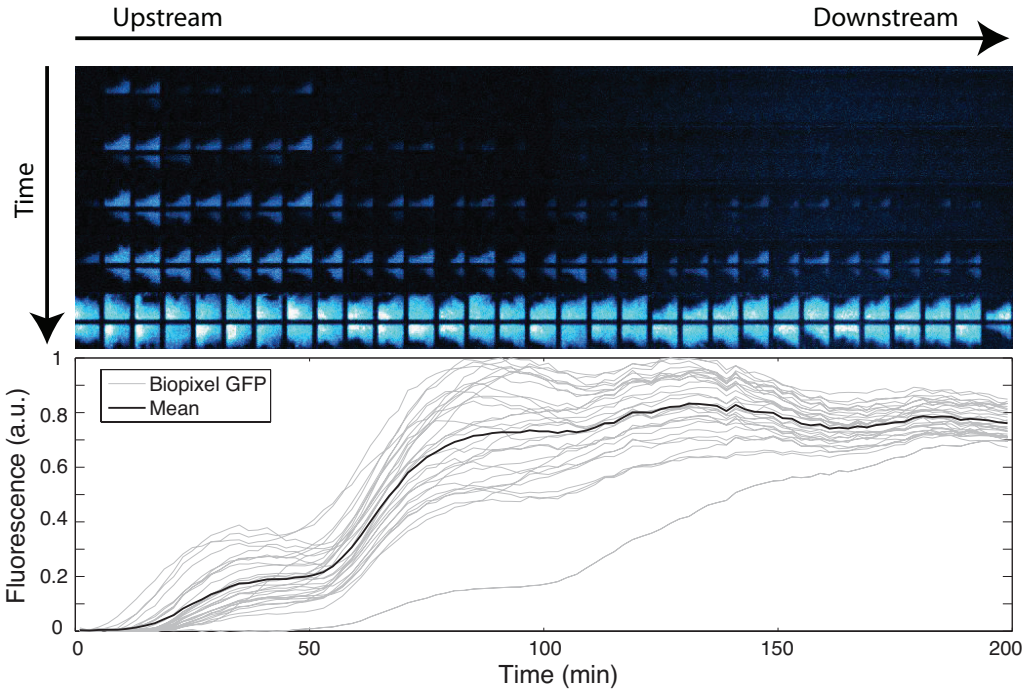

Supplementary Figure 4: SodA produces H_2O_2 internal to the cell, permanently switching the cellular redox state (oxidizing) thereby activating lux-controlled genes. Biopixels rapidly fire and lock on in a spatial wave, far earlier than is typical for colonies of this size. The propagation of ON biopixels suggests that colonies are capable of activating those nearby via migrating H_2O_2 species.

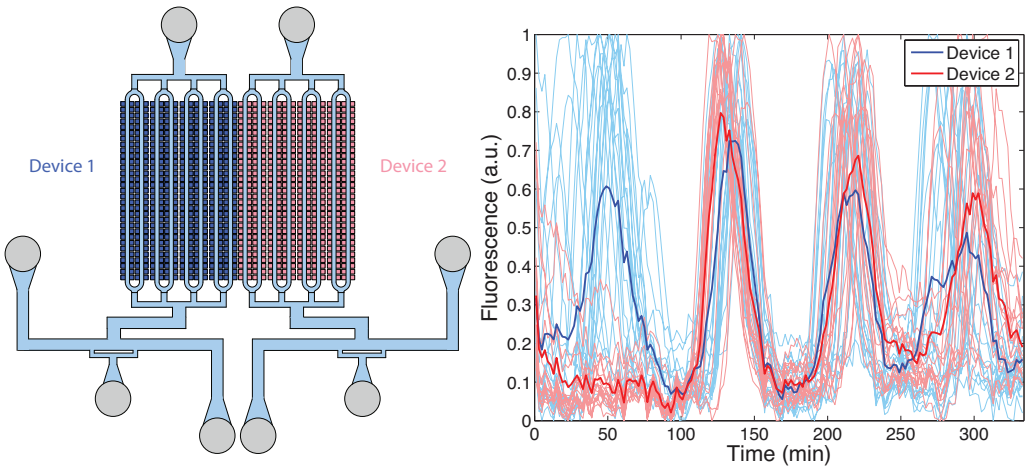

Supplementary Figure 5: Synchronized oscillations occur across 2 fluidically isolated devices held in close proximity. In this experiment, the devices were started at different times yet become synchronized. Since these devices share no common fluid sources or sinks, this confirms that synchronization is mediated by vapor species.

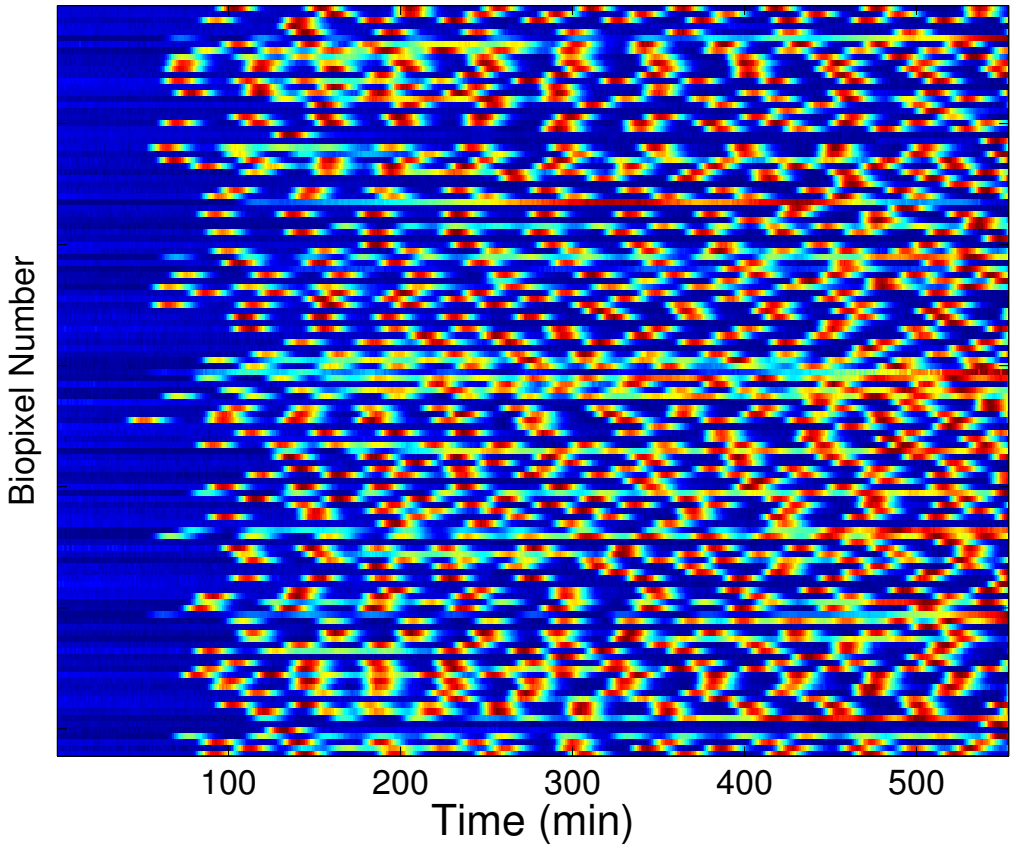

Supplementary Figure 6: Heatmap of trajectories extracted from low fluorescence intensity control (Suppl. Movie 9) when NDH-2 plasmid is not present. Biopixels oscillate individually but fail to synchronize.

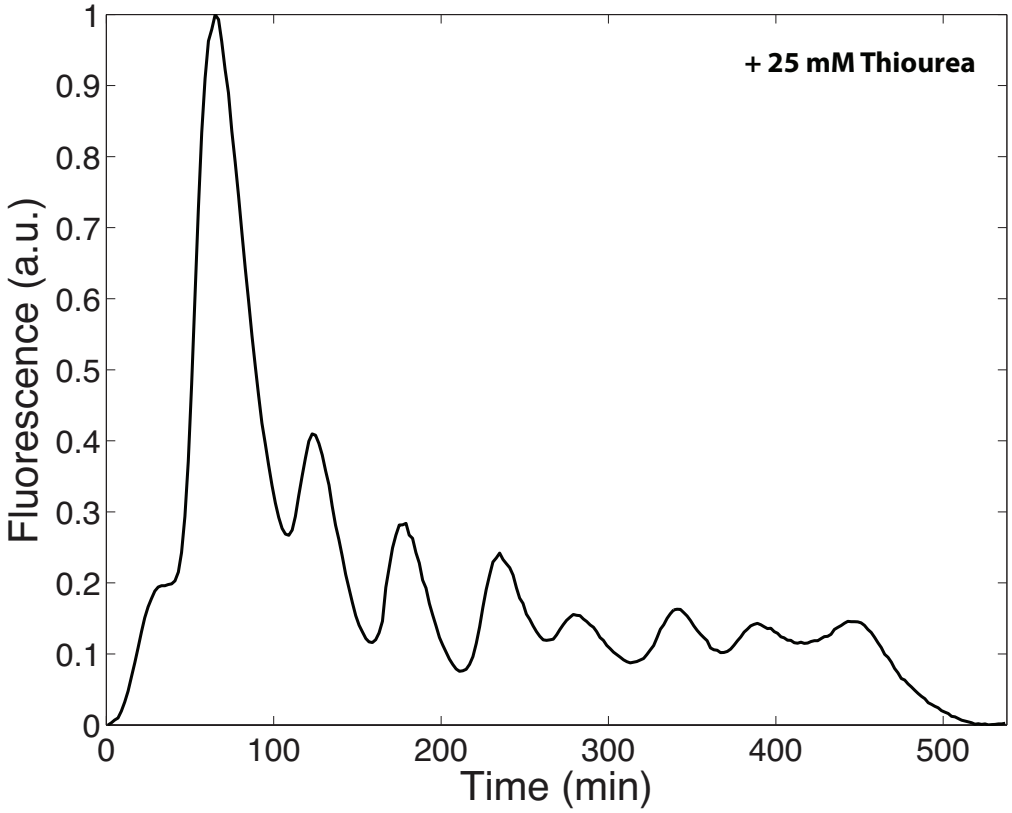

Supplementary Figure 7: The introduction thiourea, a potent radical quencher, produces decaying synchronized oscillations across a population of biopixels. Because radical species are precursors for H_2O_2 , eliminating them lowers the production of H_2O_2 and therefore dampens the oscillations. Colonies are still able to synchronize because, while thiourea eliminates radicals within cells, it does not prevent H_2O_2 from diffusing between cells.

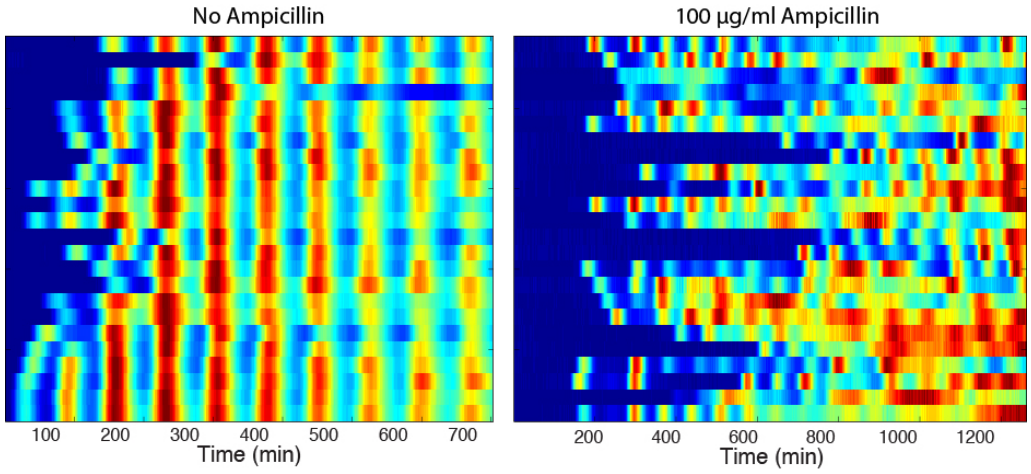

Supplementary Figure 8: Synchronization is prevented when 100 μg/ml Ampicillin is used in the media. The constructs, strains, and experimental conditions are otherwise identical.

Data Analysis

Fluorescence data was obtained by importing fluorescent images into ImageJ and subtracting cell signal from background signal. Oscillatory period was taken to be the average of peak-to-peak and trough-to-trough distance, calculated using a MATLAB script. The data represented in Fig. 1d and 2b-d were collected by stitching 4 images taken at 4X magnification. The mean trajectory in Fig. 1d was found by averaging 373 individual biopixel trajectories, of which 20 are shown. Biopixel trajectories were extracted from image series using a MATLAB script, where a bright field image of the corresponding array was used to generate a mask. The data shown in Fig. 2c was measured over 4 separate experiments using 10-30 oscillatory periods per data point.

Sensor calibration curve (Fig. 2c, bottom) was generated using a series of 2-population ttests comparing the experimental datasets to randomly generated new sample sets. The mean of generated sets was decremented until the ttest failed with $\alpha = 95\%$, indicating the lowest period that could be associated with that arsenite concentration. We repeated this process for each arsenite level and fit the points with a quadratic since we expected it to take the inverse shape of the period vs. arsenite measurements.

Microscopy and Microfluidics

We used a microscopy system similar to our recent studies (1), with the addition of a high-sensitivity Andor DU-897 EMCCD camera. Fluorescent images were taken at 4X every 30 seconds using the EMCCD camera (20ms exposure, 97% attentuation) or 2 minutes (2s exposure, 90% attenuation) using a standard CCD camera to prevent photobleaching or phototoxicity.

In each device, *E. coli* cells are loaded from the cell port while keeping the media port at sufficiently higher pressure than the waste port below to prevent contamination (Suppl. Fig 8). Cells were loaded into the cell traps by manually applying pressure pulses to the lines to induce a momentary flow change. The flow was then reversed and allowed for cells to receive fresh media with 0.075% Tween which prevented cells from adhering to the main channels and waste ports.

To measure fluid flow rate before each experiment, we measured the streak length of fluorescent beads (1.0 μm) upon 100 ms exposure to fluorescent light. We averaged at least 1,000 data points for each.

We constructed several microfluidic devices over the course of the study. The trap dimensions were always 100 μm x 85 μm x 1.65 μm high, which we previously found to be optimal for oscillator function, except when size was varied to study dynamic interactions. Spacing between traps was 25 μm, except in devices designed to study the effects of increasing separation distance between traps. For sensor array devices, we constructed 500 and 12,000 trap arrays as well as a tandem device which holds two 150 trap arrays in close proximity (25 μm) without sharing fluid sources or sinks.

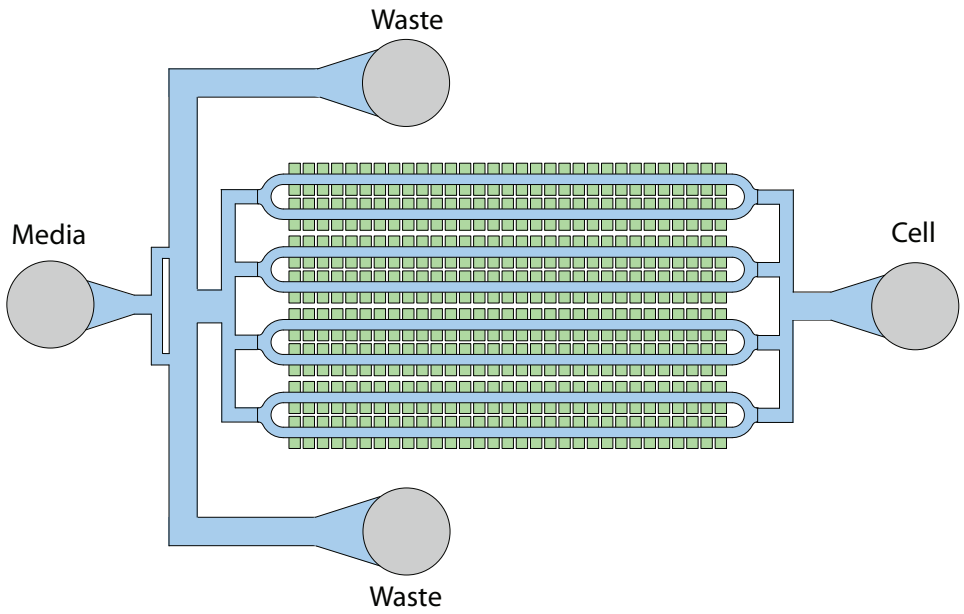

Supplementary Figure 9: Primary microfluidic device used for this study. Media containing variable arsenite concentration is fed through the cell port, flowing past the biopixel array into the cell and waste ports. During loading, pressure is increased at the cell port and decreased at the waste ports to reverse the flow, allowing cells to pass by the trapping regions. Other microfluidic devices used have the same layout with trap number, separation, and size varied.

Modeling

To model the dynamics of the quorum-sensing oscillator, we used our previously described model for intracellular concentrations of LuxI (I), AiiA (A), internal AHL (H_i), and external AHL (H_e) (1),

$$\frac{\partial A}{\partial t} = C_A[1-(d/d_0)^4]\ G(\alpha,\tau) - \frac{\gamma_A A}{1+f(A+I)} \quad (1)$$

$$\frac{\partial I}{\partial t} = C_I[1-(d/d_0)^4]\ G(\alpha,\tau) - \frac{\gamma_I I}{1+f(A+I)} \quad (2)$$

$$\frac{\partial H_i}{\partial t} = \frac{bI}{1+kI} - \frac{\gamma_H A H_i}{1+gA} + D(H_e - H_i) \quad (3)$$

$$\frac{\partial H_e}{\partial t} = -\frac{d}{1-d}D(H_e - H_i) - \mu H_e + D_1\frac{\partial^2 H_e}{\partial x^2} \quad (4)$$

In the original model, the concentration of the constitutively produced LuxR protein R was assumed constant. In the ON/OFF threshold arsenic biosensor circuit, LuxR production is induced by arsenic, which we model by the equation

$$\dot{R} = \frac{\alpha_c A}{(A_0+A)} - \gamma_R R \quad (5)$$

in which the LuxR expression from the arsenic promoter follows a standard saturating function of the arsenic concentration A. Accordingly, we modified the Hill function for Lux promoter to include the explicit dependence on R:

$$G(\alpha,\tau) = \frac{\delta + \alpha(R_\tau H_\tau)^2}{1+k_1(R_\tau H_\tau)^2} \quad (6)$$

For modeling the period-modulating sensor, we modified the equation for LuxI (2) to include additional production from the arsenic promoter,

$$\dot{I} = C_I[1-(d/d_0)^4]G(\alpha,\tau) + \frac{\alpha_c A}{(A_0+A)} - \frac{\gamma_I I}{(1+f(A+I)} \quad (7)$$

The following additional parameters were used for the biosensor simulations: $\alpha_c = 50$, $A_0 = 2$, $\gamma_R = .1$.

Arsenic levels were swept across the dynamic range of the arsenic promoter to produce the curve in Fig. 2c. The period for each arsenic level was calculated from the peak-to-peak average of 15 oscillatory periods.

To model the spatial synchronization of oscillating colonies across a microfluidic array, we generalized a simplified "degrade-and-fire" model (6). The delay-differential equation

$$\dot{X}_{i,j} = \frac{\alpha(1+\nu P_{i,j,\tau_2})}{(1+\frac{X_{i,j,\tau_1}}{C_0})^2} - \frac{\gamma X_{i,j}}{k+X_{i,j}} \quad (8)$$

describes oscillations of individual biopixel $\{i,j\}$ as a combined effect of production and delayed autorepression (first term in the r.h.s.) of the colony-averaged LuxI concentration $X_{i,j}$ and its enzymatic degradation by ClpXP (second term). Unlike (6), the first (production) term in Eq. 8 describes both delayed auto-repression of LuxI and its delayed activation by H_2O_2 proportional to its local concentration $P_{i,j}$. Subscripts τ_1 and τ_2 indicate the delayed concentrations, $X_{i,j,\tau_1}(t) = X_{i,j}(t-\tau_1)$ and $P_{i,j,\tau_2}(t) = P_{i,j}(t-\tau_2)$. The dynamics of $P_{i,j}$ is described by the equation

$$\dot{P}_{i,j} = \mu + \alpha_p X_{i,j} - \gamma_p P_{i,j} + \hat{S}\{P_{i,j}\} \tag{9}$$

where the first three terms describe the basal and induced production and degradation of H_2O_2. The last term models the spatial coupling of neighboring biopixels via the H_2O_2 exchange. For a square $N \times N$ array of traps, we used the following discrete diffusion form of the spatial operator,

$$\hat{S}\{P_{i,j}\} = D\Delta^{-2}[P_{i-1,j} + P_{i+1,j} + P_{i,j-1} + P_{i,j+1} - 4P_{i,j}] \tag{10}$$

Each colony is affected by the H_2O_2 produced in four neighboring colonies, two in each dimension of the array, separated by the equal distance Δ. We used the boundary condition $P_{i,j} = 0$ for the edges of the array $i,j = 0, N+1$. This represents the infinite external sink of H_2O_2 diffusing out of the microfluidic chip. The diffusion operator above can be generalized if the row spacing differs from the column spacing, or for other spatial arrangements of colonies within the biosensor.

We introduced variability among different traps by randomizing oscillator parameters for individual traps in each simulation. Specifically, LuxI (X) activation and degradation parameters ($p = \{\alpha, \gamma\}$) of each of the oscillators in the array were varied around their nominal values (p_0) as $p = p_0 + \delta$ where δ is a random number uniformly distributed between -0.25 and 0.25. We used the following dimensionless parameters for most of our simulations: $\alpha_0 = 8.25$, $\gamma_0 = 5.75$, $\nu = 1$, $\tau_1 = 10$, $\tau_2 = 20$, $C_0 = 6$, $k = 10$, $\mu = 20$, $\alpha_p = 1$, $\gamma_p = 10$, $D = 7$, $\Delta = 1$.

For the characterization of various regimes of array synchronization, 16 colonies were modeled in the 4×4 array. Scaling up the simulation with larger numbers of colonies produced equivalent results. Overproduction of H_2O_2 by expressing sodA was captured by increasing α_p 20-fold. This is consistent with expression from a pSC101m plasmid with a copy number of 20-30. Depletion of external H_2O_2 by catalase was modeled by increasing H_2O_2 degradation (γ_p) and decreasing H_2O_2 diffusion, D. In Suppl. Fig. 9 we show the variance of the concentrations $X_{i,j}$ within the array averaged over time and parameter variations. This plot demonstrates that the synchronicity among the biopixels decreases with increase of spacing among them, and for $\Delta > 5$ is completely lost.

Increasing the trap spacing Δ 2-fold while simultaneously decreasing k 4-fold allowed us to reproduce the more complex waveforms observed experimentally in our arrays. Note that changing k models the change of the trap depth. As the size of the trap decreases, the flow of media is able to more rapidly sweep away AHL and increase the effective degradation for the colony. Simulating smaller and more sparse trap sizes recovered antiphase behavior for neighboring biopixels (Suppl. Fig. 10). We also simulated the arrays with traps of two different sizes in different rows and recovered the experimental 2:1 biopixel resonance or 2:1 + antiphase behavior depending on the trap spacing (Fig. 3d, bottom).

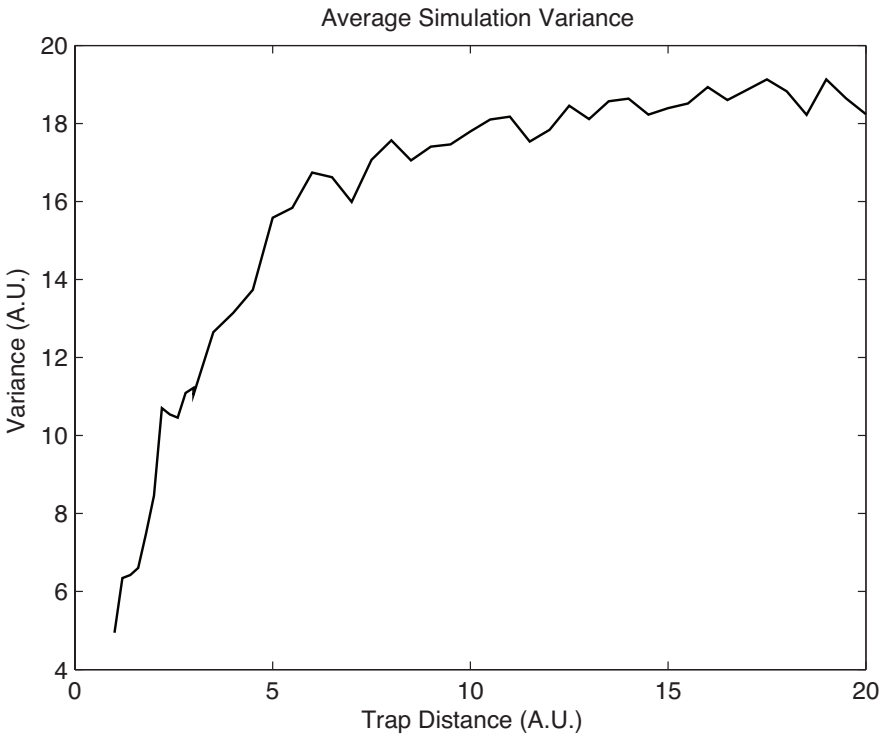

Supplementary Figure 10: Computational results depicting biopixel synchronicity as a function of trap separation distance. As biopixels are moved farther apart, the entropy increases due to decreased effective migration of H_2O_2 between colonies.

The model was also able to capture the alternating large and small amplitude oscillations observed in the ON/OFF biosensor (Suppl. Fig. 11). This behavior was seen when C_0 was increased 2-fold, capturing the decreased level of LuxR in ON/OFF experiments where it was the limiting factor for oscillations.

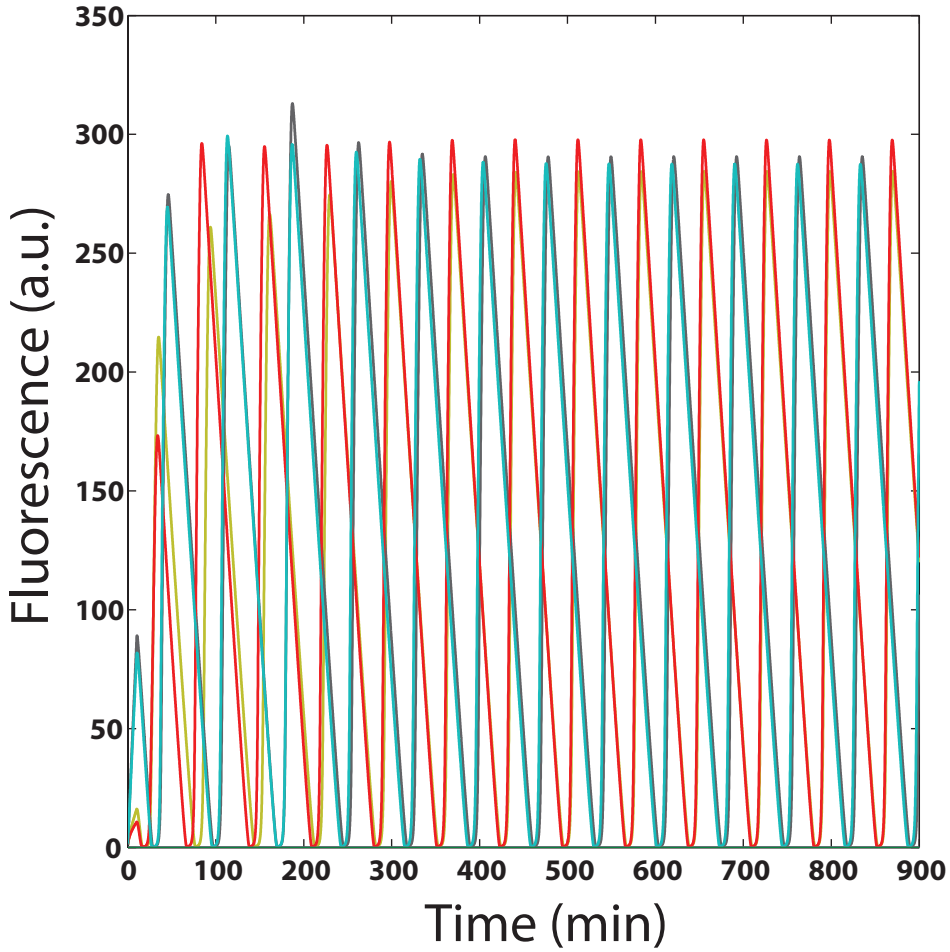

Supplementary Figure 11: Antiphase behavior of 4 neighboring biopixels having equal trap sizes and spacing $\Delta = 3$.

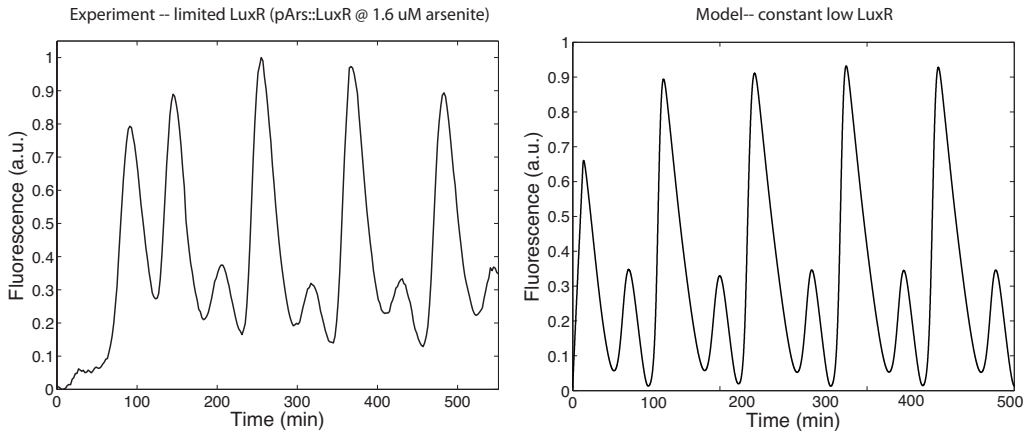

Supplementary Figure 12: Oscillations of alternating large and small amplitude when LuxR is limited in experiments and simulations. The alternating oscillations vanish when LuxR is restored to its normal level in the model. Experimentally, we were unable to build a system in which LuxR is tunable between big/small and normal amplitude regimes. This is probably due to the small dynamic range of arsenite promoter-driven output of LuxR compared to the level produced by 3 constitutively expressed copies in the original circuit.

References

[1] Danino, T., Mondragon-Palomino, O., Tsimring, L. & Hasty, J. A synchronized quorum of genetic clocks. *Nature* **463**, 326–330 (2010).

[2] Pedelacq, J.-D., Cabantous, S., Tran, T., Terwilliger, T. C. & Waldo, G. S. Engineering and characterization of a superfolder green fluorescent protein. *Nature Biotechnology* **24**, 79–88 (2006).

[3] Stocker, J. *et al.* Development of a set of simple bacterial biosensors for quantitative and rapid measurements of arsenite and arsenate in potable water. *Environ. Sci. Technol* **37**, 4743–4750 (2003).

[4] Keiler, K., Waller, P. & Sauer, R. Role of a peptide tagging system in degradation of proteins synthesized from damaged messenger rna. *Science* **271**, 990 (1996).

[5] Quan, J. & Tian, J. Circular polymerase extension cloning of complex gene libraries and pathways. *PloS one* **4**, e6441 (2009).

[6] Mather, W., Bennett, M., Hasty, J. & Tsimring, L. Delay-induced degrade-and-fire oscillations in small genetic circuits. *Physical Review Letters* **102**, 068105 (2009).